Relationships between composition and properties of (Cr/Ti)SiN and (Cr/Ti)CN alloys: an *ab initio* study

2009 J. Phys.: Condens. Matter 21 285302

(http://iopscience.iop.org/0953-8984/21/28/285302)

J. Phys.: Condens. Matter **21** (2009) 285302 (11pp) doi:10.1088/0953-8984/21/28/285302

Relationships between composition and properties of (Cr/Ti)SiN and (Cr/Ti)CN alloys: an *ab initio* study

J Houska, J E Klemberg-Sapieha and L Martinu

Department of Engineering Physics, Ecole Polytechnique, 2900, boulevard Edouard-Montpetit, Montreal, QC, H3C 3A7, Canada

E-mail: jhouska@kfy.zcu.cz

Received 13 March 2009
Published 17 June 2009
Online at stacks.iop.org/JPhysCM/21/285302

Abstract

It has previously been noted that different fcc metal nitrides exhibit different superior properties, including the high hardness of TiN and the excellent corrosion and oxidation resistance of CrN. Si and C have been added into such metal nitrides in order to tailor their functional properties. Contrary to the intensively studied TiSiN and TiCN nanocomposite and solid solution systems, much less is known about the complex relationships between the composition and the properties of CrSiN and CrCN. In fact, there is a qualitative difference between cubic spin-unpolarized materials such as TiN, and spin-polarized materials such as CrN which may exhibit a cubic/orthorhombic structural transformation. In the present work, we report *ab initio* calculations of the properties of (Cr/Ti)SiN and (Cr/Ti)CN systems of various compositions. We specifically predict the lattice constant, bulk modulus, elastic tensor, shear modulus, Young's modulus, Poisson's ratio, magnetization, electronic structure and preference towards the cubic/orthorhombic structural transformation. Knowledge of the modeled relationships allows one to tailor the material characteristics of various ternary metal nitrides for different technological applications.

(Some figures in this article are in colour only in the electronic version)

1. Introduction

Thin films of cubic transition metal nitrides, MN (M = e.g. Ti, Cr, Zr, or Nb), are of great importance as hard protective coatings. In order to further increase their hardness, wear resistance or thermal stability, other elements such as Si or C are incorporated. C replaces N in the MN network in a wide compositional range (for the corresponding experimental observations, see e.g. [1–4] (Ti) and [5, 6] (Cr)). Si replaces M in the MN network, exhibiting an 'effective solubility' which depends on the kinetic conditions during the film growth. This effective solubility can be significantly higher than the theoretical one, and contribute to the 'solid solution hardening' mechanism (for the corresponding experimental observations, see e.g. [7–11] (Ti), [12, 13] (Cr), [14] (Zr) and [15] (Nb)). Detailed data on the solid solution formation in the case of the most intensively studied TiSiN system are described in [16] for a molecular dynamics observation (Si content in MN crystals, [Si], up to 4%), and in [17] for the theoretical upper limit before amorphization of the structure ([Si] = 12%).

The resulting ternary coatings are applied in different areas of engineering and industry in order to improve the mechanical properties of surfaces. Examples of application fields are the machining and manufacturing industries, hard coatings for optics, anticorrosive and decorative coatings, and others. In parallel, these materials are also of fundamental interest with regard to understanding the relationships between their structure, electronic structure and functional characteristics.

Some characteristics, such as high hardness, wear resistance, high melting point or high chemical and thermal stability are commonly reported for all MN. On the other hand, there are also considerable variations between these compounds. First of all, there are significant differences between their magnetization (unpaired-spin density), as shown in figure 1 (for the methodology needed see section 2). TiN,

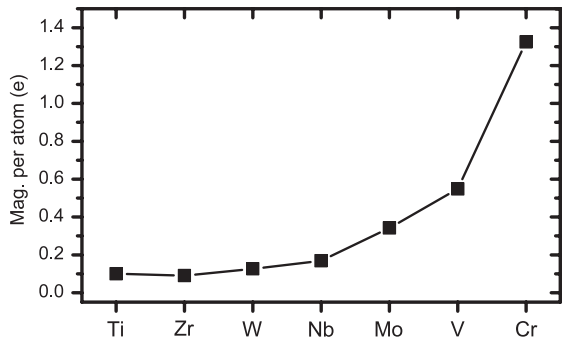

Figure 1. Zero temperature magnetization (number of unpaired spins) per atom for various metal nitrides. The line is only a guide for the eye.

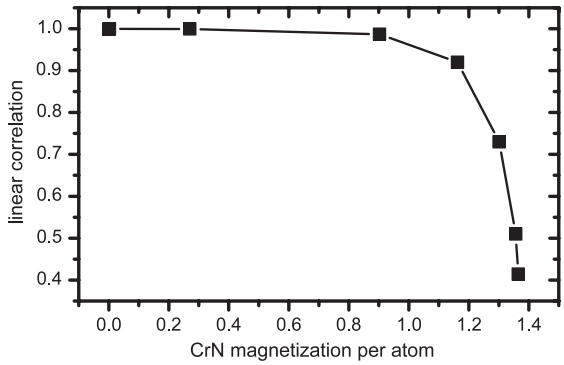

Figure 2. Relationship between (1) magnetization of CrN and (2) linear correlation between the total energies and angle (4 non-zero angles up to 6°) of the shear applied. Different magnetizations were obtained at different temperatures by varying the value of the Fermi–Dirac smearing around the Fermi energy, with the highest magnetization corresponding to the zero temperature. The shear was performed in the xy plane, perpendicular to the ferromagnetic layers, in which it takes place experimentally. A linear correlation of 1 corresponds to a preference for the cubic structure.

ZrN, or WN exhibit almost no magnetization (and can be safely studied theoretically using the paired-spin approach), which is followed by enhanced magnetization of NbN, MoN and VN, and by the highest magnetization exhibited by Cr. This corresponds to the experimentally [18] known preference of CrN to convert from a paramagnetic (PM) configuration to a double-layer antiferromagnetic (AFM) configuration ((110) ferromagnetic (FM) layers). The transition takes place slightly below room temperature (273–283 K), and it may be associated with a shear where the angle between the original cubic lattice vectors changes slightly. However, this does not take place in the case of epitaxial constraints [19]. It can be seen in figure 2 that the CrN shear occurs in the case of a magnetization of around 0.9 per atom, compared to the magnetization of almost 1.4 per atom calculated at the preferred volume (while there is higher magnetization per atom with a tensile stress and vice versa [20]). In parallel, there are known differences in material characteristics including (to compare just Ti and Cr) the higher hardness of TiN, and the excellent corrosion and oxidation resistance of CrN. Moreover, while TiN is known to be conductive (metallic-like) due to the 3d states around the Fermi level [21], CrN was shown to be a semiconductor with a narrow band gap [22].

Knowledge of the bulk modulus, B, shear modulus, G, and Young's modulus, E, as well as the Poisson's ratio, ν, plays an important role in predicting the mechanical performance of materials. In addition, knowing the values of the elastic constants, valuable information about the bonding characteristics between atoms can be provided and vice versa. For example, the resistance to elastic strain depends primarily on the valence electron density, but there is no simple rule concerning this quantity for the systems studied, and the evolution of the shear modulus (the key quantity in determining the intrinsic hardness [23]) is even more complex. Knowledge of the lattice constant, a_0, of various compositions allows one to control the stress in a lattice in the case of epitaxial growth, and to measure the material composition using x-ray diffraction (XRD). A number of theoretical results have been reported in this field, including B and a_0, for various pure MN [24], the formation energy of TiSiN [17], the shear strength and electronic structure of (pure) SiN [17, 25], the formation energy, E_f, of TiCN [26], the G (C_{44} component of the elastic tensor, C_{ij}) of TiCN [27], various elastic moduli for TiCN [28] and the characteristics of (pure) TiN [29] and CrN [30, 31].

However, there is a large gap resulting from (1) the focus of most of the research on TiSiN and TiCN, while much less data are available for CrSiN and CrCN (let alone other MN systems), and (2) the limited accuracy of either elastic properties calculated using the local density approximation (LDA) exchange–correlation (xc) functional [20, 24] (for a detailed comparison of LDA with other xc functionals for pure TiN, see [29]), or even of results calculated for CrN using the paired-spin (zero magnetization) approach [24, 30]. In order to enhance our knowledge of the composition–properties relationships in these materials, we systematically study the characteristics of (Cr/Ti)SiN and (Cr/Ti)CN alloys of various compositions by *ab initio* calculations. We determine B, a_0, C_{ij} (having 3 independent components C_{11}, C_{12} and C_{44} for the cubic structure), G, E, ν, E_f, the electronic structure and the valence electron density profiles. We focus on the comparison of Cr- and Ti-based alloys, and in the case of Cr we further calculate magnetization and the preference towards the cubic/orthorhombic structural transition. This allows one to tailor the composition of ternary metal nitrides for the required elastic, electronic or adhesive characteristics.

2. Methodology

Throughout this work, all calculations use the density functional theory (DFT) [32, 33] as implemented in the plane-wave self-consistent field (PWSCF) code [34]. Results of selected calculations were crosschecked using the Car–Parrinello molecular dynamics (CPMD) code [35]. Atom cores and inner electron shells were represented by the Vanderbilt-type ultrasoft pseudopotentials [36]. Valence electrons were described using the Kohn–Sham equations, and the exchange and correlation term was treated using the Perdew–Burke–Ernzerhof (PBE) functional [37]. The valence electron

wavefunction was expanded using a plane-wave basis set with an energy cutoff of 30 Ryd. The integration in the reciprocal space was performed using the tetrahedron method, and a Monkhorst–Pack grid of k-points (for the number of k-points, see below). For CrSiN and CrCN spin-polarized calculations, the experimentally predicted double-layer AFM configuration was used. For the cubic structure this leads to practically the same energy and lattice constant as the disordered PM configuration [38], at a significantly lower energy compared to the spin paired or the FM configuration (however, the a_0 value of 4.19 Å itself seems to be overestimated by the technique used in [38], compared to 4.14–4.16 in [31, 39, 40] and this work). At the same time, this allows (1) a more straightforward (reproducible) description of the material and (2) an improved possibility of studying phenomena characteristic only for the AFM configuration. Technically, two formally different kinds of atoms, denoted Cr↑ and Cr↓ from now on, were used in these calculations.

The effect of the distribution of Si or C atoms in a lattice, and the effect of doping by small amounts of Si or C on the material characteristics was investigated using periodic cells containing up to 64 atoms, with a k-points grid of $3 \times 3 \times 3$ for calculations of B and $5 \times 5 \times 5$ otherwise. The effect of Si or C incorporation in a broader composition range on the material characteristics (including the electronic structure) was investigated using periodic cells containing 8 atoms (16 atoms in the case of CrSiN, where Si equally replaces Cr↑ and Cr↓), with a k-points grid of $6 \times 6 \times 6$ for the calculations of B and $9 \times 9 \times 9$ otherwise.

For each material studied, B and a_0 were obtained by fitting at least 10 energies calculated at different volumes to the Birch equation of state

$$E - E_0 = 9/8BV_0([V_0/V]^{2/3} - 1)^2 + 9/16B(B' - 4)V_0 \times ([V_0/V]^{2/3} - 1)^3 + \cdots. \quad (1)$$

Here, V and V_0 are the volume and preferred (lowest-energy) volume, respectively, and B' is the pressure derivative of B. For an example of the results see section 3.1. All other elastic characteristics, electronic characteristics and the magnetization were obtained at the a_0 value calculated here. This was followed by determining C_{ij} using (a) a volume conserving monoclinic strain [41, 42], ε_{ij}:

$$\varepsilon_{12} = \delta/2, \qquad \varepsilon_{21} = \delta/2, \qquad \varepsilon_{33} = \delta^2/[4 - \delta^2] \qquad \text{(at least } 4\delta \text{ values up to } 6^\circ\text{)}, \quad (2)$$

where $E - E_0 = V_0[\frac{1}{2}C_{44}]\delta^2$, and (b) a volume conserving orthorhombic strain:

$$\varepsilon_{11} = \delta, \qquad \varepsilon_{22} = -\delta, \qquad \varepsilon_{33} = \delta^2/[1 - \delta^2] \qquad \text{(at least } 4\delta \text{ values up to } 0.06\text{)}, \quad (3)$$

where $E - E_0 = V_0[C_{11} - C_{12}]\delta^2$. For an example of the results see section 3.2. The elastic tensor components C_{11} and C_{12} were obtained from the $C_{11} - C_{12}$ difference, and the $B = (C_{11} + 2C_{12})/3$ relationship. As all the atoms sit in inversion sites (exceptions are discussed below), the fractional coordinates of the atoms were kept constant during the C_{ij} calculations.

Note that B calculated for a monocrystal can be used as a reasonable estimate of B of a polycrystalline material. On the other hand, although both C_{44} and $(C_{11} - C_{12})/2$ can be interpreted as G, we had to calculate the Reuss's and Voigt's shear moduli as an upper and lower bound, respectively, of the shear modulus of a polycrystalline material [43]:

$$G_{\min} = G_{\text{Reuss}} = 10/(8/[C_{11} - C_{12}] + 6/C_{44}) \quad \text{and} \quad G_{\max} = G_{\text{Voigt}} = (C_{11} - C_{12} + 3C_{44})/5. \quad (4)$$

As there was only a small difference (of around 5 GPa) between G_{R} and G_{V} in our calculations, we present the results as a single average, $G_{\text{RV}} = (G_{\text{R}} + G_{\text{V}})/2$. Phenomena associated with the dependence of G on the direction of shear (particularly due to the magnetization) are discussed below. E and ν can be calculated using the formulae for the (100) direction [41, 42]:

$$E_{100} = (C_{11} + 2C_{12})(C_{11} - C_{12})/(C_{11} + C_{12}) \quad \text{and} \quad \nu_{100} = C_{12}/(C_{11} + C_{12}). \quad (5)$$

For a polycrystalline material, we make an assumption for the E and ν values using the following formulae:

$$E_{\text{RV}} = 9BG_{\text{RV}}/(3B + G_{\text{RV}}) \quad \text{and} \quad \nu_{\text{RV}} = 1/2 - 1/6E_{\text{RV}}/B. \quad (6)$$

(Here $E_{100} = E_{\text{RV}}$ and $\nu_{100} = \nu_{\text{RV}}$ in the case of replacing G_{RV} by $(C_{11} - C_{12})/2$.)

For comparison, we also present values calculated from the less frequently used [42, 44] 'isotropic formulae':

$$E_{\text{iso}} = C_{44}(2C_{44} + 3C_{12})/(C_{11} + C_{44}) \quad \text{and} \quad \nu_{\text{iso}} = C_{12}/2(C_{44} + C_{12}). \quad (7)$$

The accuracy of the applied method was tested with respect to the number of k-points, wavefunction energy cutoff, density cutoff, convergence of the total energy, number of terms of the Birch equation used in the case of B, and the lattice constant used as an input parameter in the case of C_{ij}. Note that less k-points were found to be needed for convergent results in the constant-symmetry calculations of B, compared to the variable-symmetry calculations of C_{ij}. For C_{ij} calculations, a correlation of the $E(\delta^2)$ linear fit better than 0.9995 was found to be an alternative fingerprint of convergent energy differences (frequently it was better than 0.9999). In all cases, the resulting errors (<2 GPa for elastic moduli, and <0.001 Å for a_0) are sufficiently low to have no effect on the trends presented in this work.

3. Results

3.1. Effect of the distribution of Si and C atoms in the lattice and formation energies

The preferred distribution of Si in the TiN lattice was sought by calculating the volume–energy dependence (for the

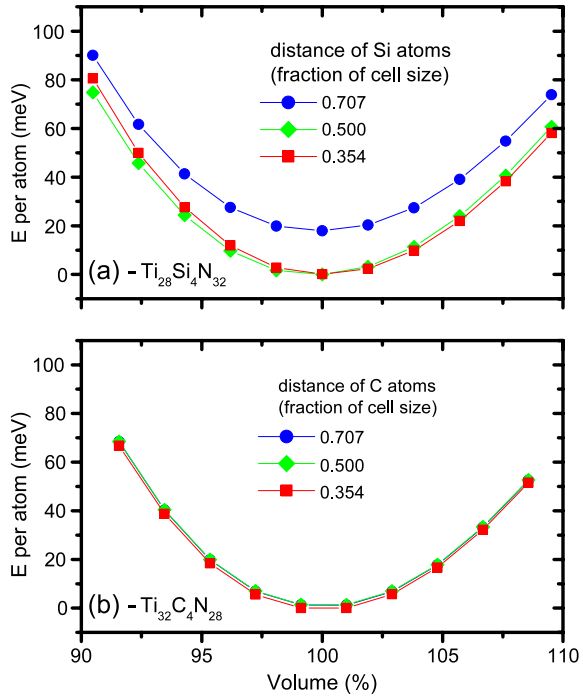

Figure 3. Dependence of the total energy on the cell volume for materials $Ti_{28}Si_4N_{32}$ (a) and $Ti_{32}C_4N_{28}$ (b). The volume is shown as a percentage of the equilibrium (lowest-energy) volume, and the energy is shown as a difference from the lowest energy obtained. Individual dependencies show data for distances of nearest Si/C atoms of $1/2\sqrt{2}$, $1/2$ and $1/\sqrt{2}$ of the 64 atom cubic cell.

resulting B and a_0, see section 3.2 below) for 7 different configurations of $Ti_{28}Si_4N_{32}$, characterized by the following fractional coordinates of the Si atoms:

(1): [0, 0, 0], [0, 0.5, 0.5], [0.5, 0, 0.5], [0.5, 0.5, 0]

(2a): [0, 0, 0], [0.5, 0.5, 0], [0.5, 0.5, 0.5], [0, 0, 0.5]

(2b): [0, 0, 0], [0, 0, 0.5], [0.5, 0.5, 0.5], [0, 0.5, 0.5]

(2c): [0, 0, 0], [0, 0, 0.5], [0.5, 0.5, 0.5], [0, 0.5, 0.5]

(3a): [0, 0, 0], [0, 0.25, 0.25], [0.5, 0.5, 0.5], [0.5, 0.75, 0.75]

(3b): [0, 0, 0], [0, 0.25, 0.25], [0.5, 0.5, 0.5], [0.75 0.75 0.5]

(3c): [0, 0, 0], [0.25, 0.25, 0], [0, 0.25, 0.25], [0.25, 0, 0.25].

Configurations 1, 2a–c and 3a–c are characterized by the distances of the nearest Si atoms of $1/\sqrt{2}$, $1/2$ and $1/(2\sqrt{2})$, respectively, in terms of the cell size. In configurations 2a and 3a, the lines connecting the nearest Si atoms are parallel, in configurations 2b and 3b there are points where 2 such lines intersect, and in configurations 2c and 3c there are points where 3 such lines intersect. Figure 3(a) shows that configurations 2 and 3 exhibit a significantly lower energy (although the solid solutions are still metastable) than configuration 1. On the other hand, there are only negligible differences in the energies exhibited within configurations 2a-c, and within configurations 3a–c (not shown). In other words, the preference investigated is given only by the distance of the nearest Si atoms. We selected configuration 2 for the following calculations (i.e. the distance of the nearest Si atoms was $1/2$ of the 64 atom cell for any composition) and used it not only for TiSiN but also for CrSiN. This choice (contrary to the energetically equivalent configuration 3) not only simplifies C_{ij} calculations by inserting all atoms into inversion sites, but it also allows one to replace the same number of Cr↑ and Cr↓ atoms by Si (in case of lines connecting the nearest Si atoms being perpendicular to the FM layers). Equivalent calculations were also performed for the $Ti_{32}C_4N_{28}$ material (see figure 3(b)). From the overlapping dependencies it can be seen that, contrary to the Si-containing material, there is no energy penalty for the most isolated (configuration 1) C atoms in the C-containing material. This result is not surprising due to the solubility of C in TiN, and it allows us to use the same distribution (minimal distances) of C atoms in the lattice as for the Si atoms.

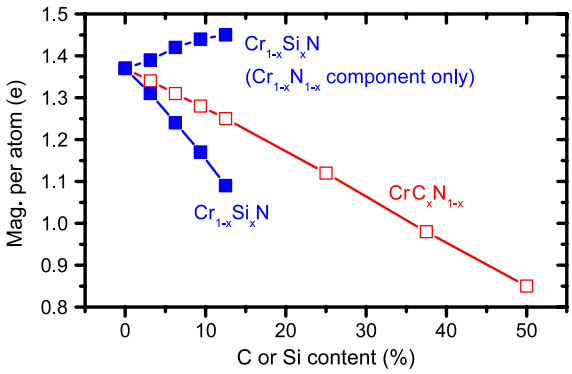

Figure 4. Absolute value of magnetization per atom for the CrC_xN_{1-x} (empty symbols) and $Cr_{1-x}Si_xN$ (full symbols) materials.

The formation energy of $Ti_{75}Si_{25}N$ (positive in case of an energy penalty for the metastable solid solution) was found to be 0.25 eV/atom with respect to $TiN + Si_3N_4 + Si$, and 0.06 eV/atom with respect to $TiN + SiN$. The formation energy of $Cr_{75}Si_{25}N$ was found to be 0.12 eV/atom with respect to $TiN + Si_3N_4 + Si$, and −0.07 eV/atom with respect to $CrN + SiN$. This shows that the solid solution formation is (under same kinetic conditions) even more likely for CrSiN compared to TiSiN. Nevertheless, for comparison purposes the effect of Si and C incorporation into TiN and into CrN is shown up to same percentages in the following sections.

3.2. Magnetization of the CrC_xN_{1-x} and $Cr_{1-x}Si_xN$ materials of various compositions

Figure 4 shows the absolute value of magnetization per atom for the CrC_xN_{1-x} and $Cr_{1-x}Si_xN$ materials (same convention—empty red symbols for CrC_xN_{1-x}, and full blue symbols for $Cr_{1-x}Si_xN$—is used in all figures from now on). For selected compositions, corresponding values of the magnetization associated with individual atom types are provided in table 1.

For CrC_xN_{1-x}, the magnetization per atom linearly decreases with increasing x over the full compositional range from 1.35 (see also figure 1) to 0.85. This is due to the lower magnetization of Cr atoms when they have more C (instead of N) atoms among their nearest neighbors. Interestingly,

Table 1. Absolute value of magnetization of individual atom types for materials CrN, $CrC_{0.25}N_{0.75}$ and $Cr_{0.75}Si_{0.25}N$. For Cr, two individual values for (1) Cr atoms nearest to the C or Si and (2) the other Cr atoms are provided. The C magnetization is ↑ if there are more Cr↓ atoms among its nearest neighbors and vice versa. The (small) Si magnetization is ↑ if it replaced an Cr↓ atom and vice versa.

Material	Element	Magnetization (e/at.)
CrN	Cr	2.65
	N	0.02
$CrC_{0.25}N_{0.75}$	Cr close to C	2.34
	Cr far from C	2.63
	C	0.15
	N	<0.02
$Cr_{0.75}Si_{0.25}N$	Cr close to Si	2.79
	Cr far from Si	2.76
	Si	0.003
	N	<0.03

there is a non-zero magnetization of the C atoms due to their interaction with Cr. This leads to (1) only a moderate decrease of the total magnetization per atom, and (2) breaking of symmetry in calculations with an odd number of C atoms, i.e. a doubled number of atoms per cell in calculations where the effect of C magnetization is not negligible.

For $Cr_{1-x}Si_xN$, the magnetization per atom decreases with increasing x with more than a two times steeper slope compared to CrC_xN_{1-x}. In this case the decrease is obvious, as the material consists of $Cr_{1-x}N_{1-x}$ and non-magnetized Si_xN_x. However, the magnetization is higher than that which would correspond to the mixing rule, as the magnetization of all Cr atoms (i.e. not only nearest neighbors of Si) slightly increases with increasing x.

The changing magnetization has a significant effect on the behavior of materials in shear. For CrN, the squares in figure 5(a) confirm the (low-temperature) preference towards shear in the xy plane, perpendicular to the FM layers (see the broad energy minimum around 3°, for the resulting linear correlation see figure 2). As figure 5(a) shows, a lower magnetization resulting from C or Si addition leads to (1) a lower depth of the energy minima (indicating a shift of the transition to lower temperatures), and to (2) lower values of the shear angles. On the other hand, figure 5(b) shows a linear energy dependence on the shear angle (as for non-magnetized TiSiN and TiCN, with a correlation better than 0.9999) in the case of shear in the xz (or yz) plane, which is not affected by the spin ordering.

3.3. Lattice constants and elastic properties of binary nitrides

The lattice constants and elastic properties of binary TiN and CrN are shown in table 2. For TiN, the calculated values including $B = 274$ GPa, $C_{11} = 584$ GPa, $C_{12} = 119$ GPa, $C_{44} = 167$ GPa, $E_{RV} = 464$ GPa and $\nu_{RV} = 0.22$ are in good agreement with the results calculated previously using the same level of theory [29] ($B = 278$ GPa, $C_{11} = 598$ GPa, $C_{12} = 118$ GPa and $C_{44} = 159$ GPa) as well as with the results obtained experimentally for sputter-deposited TiN [45] ($E = 427$ GPa and $\nu_{RV} = 0.23$). For a more detailed

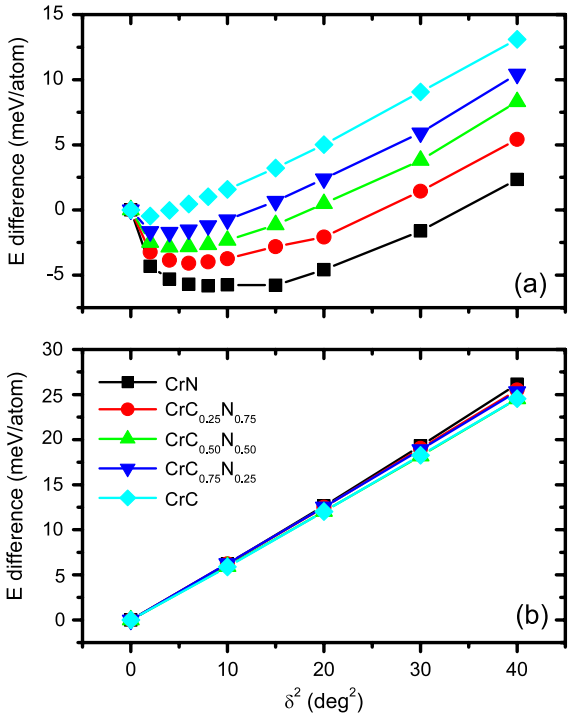

Figure 5. Energy penalty for the shear of CrC_xN_{1-x} materials spin polarized in the (001) direction as a function of the shear angle. The shear was performed in the xy plane (panel (a)) and in the xz plane (panel (b)). In panel (a), data for the $CrC_{75}N_{25}$ material almost overlap with data for the $Cr_{75}Si_{25}N$ material (not shown).

overview of B and C_{ij} obtained using various techniques, see [29]. The experimental values of E and ν support the use of E_{RV} and ν_{RV} for materials with a disordered grain orientation, while directional values such as E_{100} and ν_{100} (544 GPa and 0.17, respectively, for TiN) are useful for the characterization of materials exhibiting epitaxial growth and/or a columnar structure. On the other hand, E_{iso} (and consequently ν_{iso}) values (157 GPa and 0.21, respectively, for TiN) are clearly not preferred.

Significantly less theoretical or experimental data are available for CrN compared to TiN, except for a_0 (4.14–4.16 Å [31, 39, 40], both measured and calculated, compared to our 4.156 Å) and B (calculated 245 GPa [31], compared to our value of 241 GPa). There is only a limited agreement in the (in this case only experimental) literature concerning other elastic constants, this includes E values of 190 ± 50 GPa [46], 230 GPa [47], 312 GPa [31], 405 GPa [40], or 358–486 GPa [48], compared to our value of $E_{RV} = 379$ GPa (at $E_{100} = 466$ GPa and $E_{iso} = 125$ GPa). ν was estimated to be 0.23 and 0.25 ± 0.01 in [49] and [31], respectively, compared to our value of $\nu_{RV} = 0.24$ (at $\nu_{100} = 0.18$ and $\nu_{iso} = 0.22$). On the other hand, a frequently used value of $\nu = 0.29$ provided in [47] seems to be overestimated.

It can be seen in table 2 that very similar results were obtained independently of (1) the Brillouin zone integration technique, and (2) the direction of the Cr collinear spins. Moreover, very similar CrN elastic constants (and the magnetization) were also obtained after allowing the atoms to relax, except the Cr lattice constant which decreased by

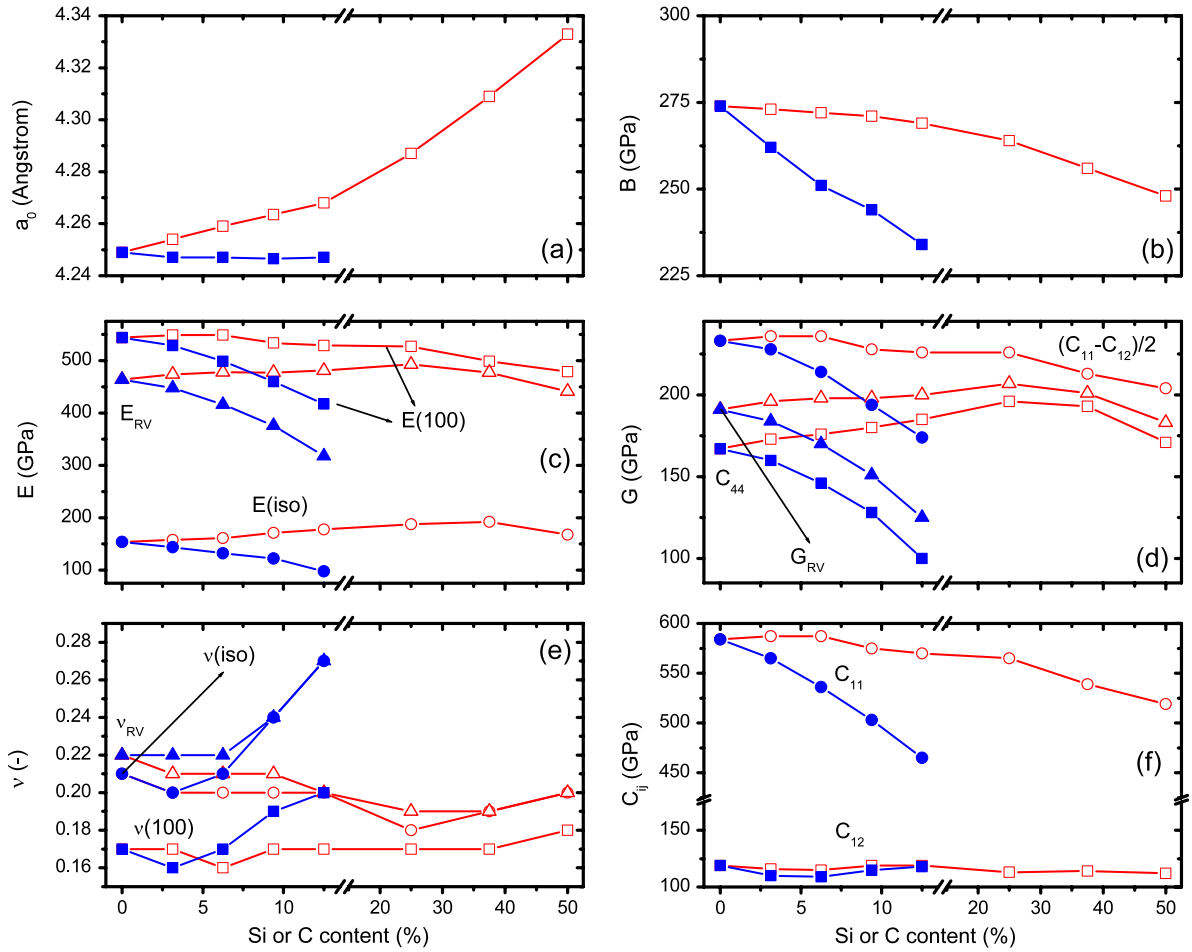

Figure 6. Lattice constants (panel (a)), bulk, Young's and shear moduli (panels (b)–(d), respectively), Poisson's ratio (panel (e)) and elastic tensor components (panel (f)) for the TiC_xN_{1-x} (empty symbols) and $Ti_{1-x}Si_xN$ (full symbols) materials.

Table 2. Characteristics of fcc-TiN and fcc-CrN, and the effect of (1) the Brillouin zone integration technique (tetrahedral, or Fermi–Dirac smearing around Fermi level), (2) the magnetic state of CrN (AFM, AFM with spins turned by 90° in the ferromagnetic layers, or nonmagnetic), and (3) the relaxation of the atomic positions (in a perpendicular direction to the CrN ferromagnetic layers). For the fictitious nonmagnetic CrN configuration the energy in shear does not change linearly with δ^2.

Material	Configuration/technique	a_0 (Å)	B (GPa)	C_{11} (GPa)	C_{12} (GPa)	C_{44} (GPa)	G_{RV} (GPa)	E_{RV} (GPa)	ν_{RV} (—)
TiN	Tetrahedra	4.249	274	584	119	167	191	464	0.22
TiN	F-D smearing	4.249	275	582	122	168	191	464	0.22
CrN	AFM, tetrahedra	4.156	241	502	111	130	153	379	0.24
CrN	AFM, F-D smearing	4.156	242	502	112	130	153	379	0.24
CrN	AFM, spins turned by 90°	4.156	241	506	108	130	154	381	0.24
CrN	AFM, relaxation of at.pos.	4.141	240	533	93	117	151	375	0.24
CrN	Nonmagnetic	4.050	322	565	200				

0.015 Å (which may or may not take place in reality after spin ordering resulting from material cooling, depending on its epitaxial stabilization). The atomic shifts were found to be 0.10 Å in a perpendicular direction to the CrN FM layers (Cr atoms towards layers with the opposite magnetization, and N atoms towards layers with the same magnetization). The table shows the key importance of introducing the spin polarization into the calculations, as the B value calculated for the fictitious non-magnetized CrN is as high as 322 GPa (let alone the 361 GPa [24] obtained using the LDA xc functional). In other words, the magnetization significantly decreases B (and increases $a0$), compared to what would correspond to the trend found for non-magnetized metal nitrides [24] (B increasing with valence electron density). The effect of this phenomenon on the trends exhibited by CrC_xN_{1-x} and $Cr_{1-x}Si_xN$ are discussed in section 3.4.

3.4. Lattice constants and elastic properties of ternary nitrides

The lattice constants and elastic properties of the TiC_xN_{1-x} and $Ti_{1-x}Si_xN$ materials are shown in figure 6. Results obtained for

the TiC_xN_{1-x} material at x increasing from 0 to 1 include:

(1) a_0 increasing from 4.249 to 4.333 Å,
(2) B decreasing from 274 to 248 GPa,
(3) G_{RV} changing from 191 to 183 GPa with a maximum of 207 GPa at $x = 0.5$ and C_{44} changing from 167 to 171 GPa with a maximum of 196 GPa at $x = 0.5$,
(4) E_{RV} changing from 464 to 441 GPa with a maximum of 493 GPa at $x = 0.5$,
(5) ν_{RV} slightly changing from 0.22 to 0.20 with a minimum of 0.19 at $x = 0.50$–0.75, and
(6) C_{11}, C_{12} and $(C_{11}-C_{12})/2$ almost constant up to x around 12.5 and then decreasing from 584 to 519 GPa, from 119 to 112 GPa, and from 236 to 204 GPa, respectively.

Comparison with trends calculated using the full potential linearized augmented plane-wave method [28] (FLAPW, contrary to the pseudopotential method used in this work) reveals an excellent qualitative agreement, with the largest quantitative difference of the FLAPW approach being systematically lower (by 5–12 GPa) C_{44} values. Decreasing values of B can be explained by a decreasing number of bonding (valence) electrons per atom (from 4.5 to 4.0). The non-monotonous behavior of C_{44} (and consequently of the C_{44}-dependent characteristics) has been explained in [27] for various metal nitrides by the filling of σ (non-metal p)/(metal d) orbitals, stable against shear deformations, which take place at about 4.2 valence electrons per atom (i.e. at $x = 0.6$ for TiC_xN_{1-x}). However, there is no such phenomenon for the other shear modulus $(C_{11} - C_{12})/2$, which controls strain deformations. Changes of a_0, useful for determining the C content in the crystals by x-ray diffraction, are slightly faster than linear and can be expressed as $a_{0(TiCxN1-x)} - a_{0(TiN)}(\text{Å}) = 6.84 \times 10^{-4}x + 1.47 \times 10^{-6}x^2$ (with a correlation of 0.9998).

Results obtained for the $Ti_{1-x}Si_xN$ material at x increasing from 0 to the 0.25 limit [17] include:

(1) an almost constant a_0 of 4.247–4.249 Å,
(2) B decreasing from 274 to 234 GPa,
(3) G_{RV} decreasing from 191 to 125 GPa and C_{44} decreasing 167 to 100 GPa,
(4) E_{RV} decreasing from 464 to 318 GPa,
(5) ν_{RV} almost constant up to $x = 12.5$ and then increasing from 0.22 to 0.27,
(6) C_{11} and $(C_{11} - C_{12})/2$ decreasing from 584 to 465 GPa and from 236 to 174 GPa, respectively, and
(7) C_{12} having a shallow minimum—a decrease from 119 to 109 followed by an increase to 118 GPa—at $x = 12.5$.

The a_0 changes are below the x-ray resolution limit in this case. On the other hand, both the decreases of all elastic moduli values (except C_{12}) and the increase of Poisson's ratio values have much steeper slopes compared to the changes exhibited by TiC_xN_{1-x} (making them observable experimentally even at low x). At a constant number of valence electrons per atom ($3d^24s^2$ for Ti and $3p^23s^2$ for Si), the material is weakening with increasing x due to the replacement of the (deformation-resisting states derived from) 3d Ti electrons by 3p Si electrons. At the same time, there are not enough valence electrons to form a fully directional bonding structure as, for example, in Si_3N_4.

The lattice constants and elastic properties of CrC_xN_{1-x} and $Cr_{1-x}Si_xN$ materials are shown in figure 7. In panel 7(a), a_0 of CrC_xN_{1-x} is shown both before the relaxation resulting from the low-temperature AFM spin ordering (in order to facilitate comparison with an experiment, as it corresponds both to unrelaxed AFM and to PM configuration [38]) and after the relaxation. The figure shows that the a_0 difference (and, consequently, the compressive stress resulting from the spin ordering) decreases with increasing x. It can be seen from comparison of figures 5 and 6 that the observed quantities exhibit different behaviors resulting from the addition of Si or C to TiN and to CrN. This is predominantly due to the effect of Si and C on the CrN magnetization (see section 3.2), which affects the characteristics observed (see section 3.3). In particular, results obtained for the CrC_xN_{1-x} material at x increasing from 0 to 1 include:

(1) a_0 decreasing (contrary to TiC_xN_{1-x}) from 4.157 to 4.102 Å,
(2) B slightly increasing from 241 to 247 GPa,
(3) G_{RV}, C_{11}, C_{44}, E_{RV} and ν_{RV} almost constant around 151 GPa, 499 GP, 129 GPa, 376 GPa, and 0.24–0.25, respectively,
(4) C_{12} slightly increasing from 111 to 122 GPa, and consequently,
(5) $(C_{11} - C_{12})/2$ slightly decreasing from 196 to 187 GPa.

Due to the decreasing magnetization per atom resulting from C addition (see table 1), both the negative difference of B and the positive difference of a_0, compared to the non-magnetized configuration (see table 2), are smaller, leading to a higher B (and the properties depending on B) and lower a_0 compared to what one would expect from the comparison with TiC_xN_{1-x} at the same x. Changes of a_0 are very linear (correlation of 0.999) in this case, and they can be expressed as $a_{0(CrCxN1-x)} - a_{0(CrN)}(\text{Å}) = -5.59 \times 10^{-4}x$. Due to the two extra valence electrons of Cr ($3d^54s^1$) compared to Ti ($3d^24s^2$), the phenomenon which causes the extremal behavior of the shear moduli (maxima at 4.2 valence electrons per atom) shown in figure 5 does not take place here.

The trends obtained for the $Cr_{1-x}Si_xN$ material are qualitatively comparable to that obtained for $Ti_{1-x}Si_xN$. However, their slopes (in % of the original values) are significantly lower. In particular, up to the same $x = 0.25$ limit they include:

(1) an almost constant a_0 of 4.154–4.158 Å,
(2) B decreasing from 241 to 225 GPa,
(3) G_{RV} changing from 153 to 142 GPa with a tiny peak of 156 GPa at $x = 0.03$ and C_{44} changing from 130 to 132 GPa with a tiny maximum of 137 GPa at $x = 0.03$,
(4) E_{RV} decreasing from 384 to 352 GPa,
(5) ν_{RV} almost constant of 0.23–0.24,
(6) C_{11} and $(C_{11} - C_{12})/2$ decreasing from 502 to 437 GPa and from 196 to 159 GPa, respectively, and
(7) C_{12} slightly increasing from 111 to 119 GPa.

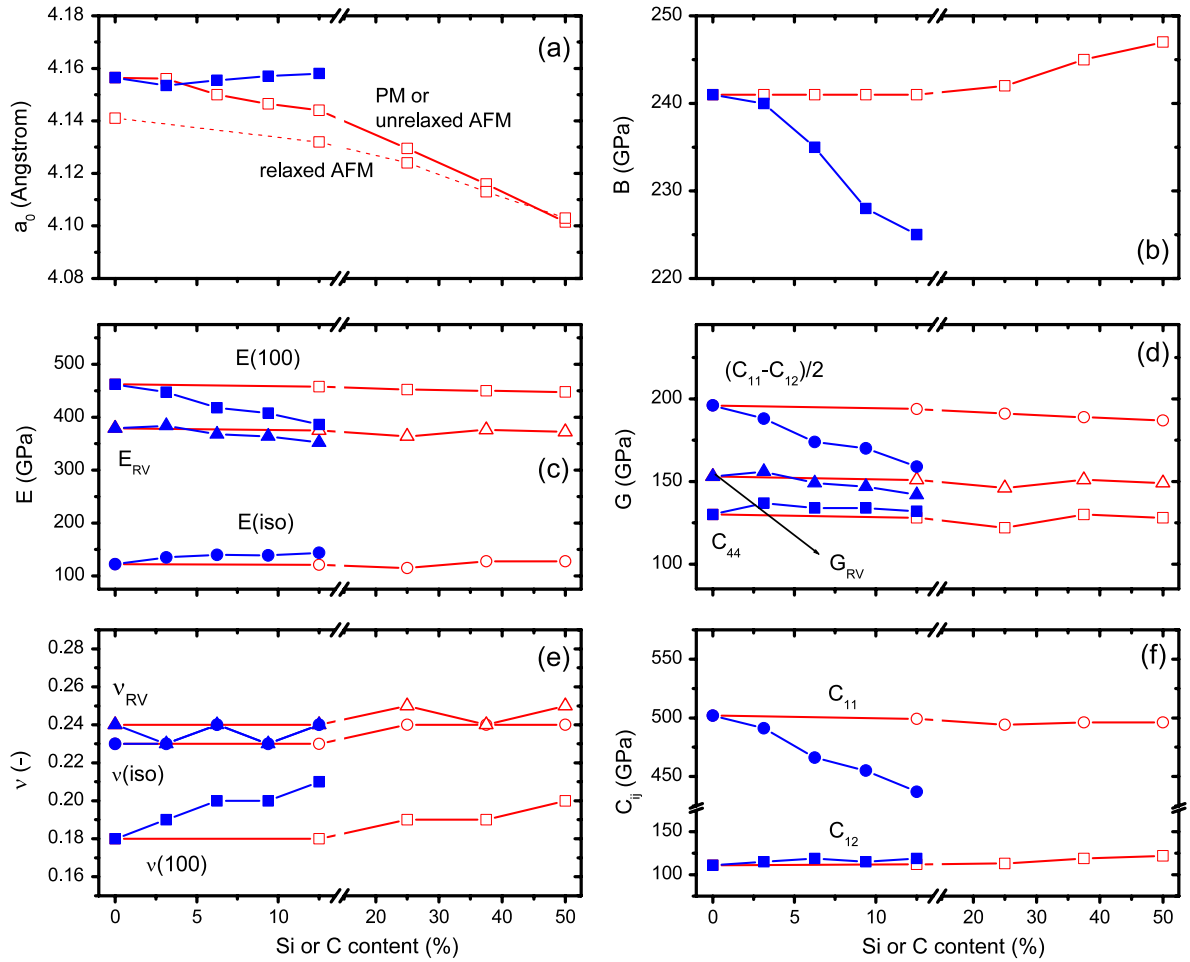

Figure 7. Lattice constants (panel (a)), bulk, Young's and shear moduli (panels (b)–(d), respectively), Poisson's ratio (panel (e)) and elastic tensor components (panel (f)) for CrC_xN_{1-x} (empty symbols, solid line), CrC_xN_{1-x} after a relaxation resulting from AFM spin ordering (panel (a) only—empty symbols, dashed line) and $Cr_{1-x}Si_xN$ (full symbols) materials.

Interestingly, despite the decreasing number of valence electrons per atom ($3d^54s^1$ for Cr compared to $3p^23s^2$ for Si), below $x = 0.25$, $Cr_{1-x}Si_xN$ is weakening less than $Ti_{1-x}Si_xN$ where the number of valence electrons is constant. While B, G_{RV} and E_{RV} are much higher for $Ti_{1-x}Si_xN$ at $x = 0$, B becomes almost the same and the other quantities higher for $Cr_{1-x}Si_xN$ at $x = 0.25$. Similar to the CrC_xN_{1-x} case, this can be explained by the higher B (and properties depending on B), compared to what one would expect from the comparison with $Ti_{1-x}Si_xN$ at the same x, due to the decreasing magnetic character of the material (see section 3.2). However, as both $Ti_{1-x}Si_xN$ and $Cr_{1-x}Si_xN$ materials become SiN at $x = 1$, a sharper decrease of elastic moduli should be expected for the fictitious high-x $Cr_{1-x}Si_xN$ (where the magnetization changes are of a smaller importance due to low Cr content).

3.5. Electron density distribution and electronic structure

The effect of the material composition on the formation of directional bonds and on the distribution of electron density (the sum of both spin up and spin down in the case of Cr) is shown in figures 8 and 9. Figure 8 shows the electron density along the interatomic CrN, CrC and SiN bonds (linkages).

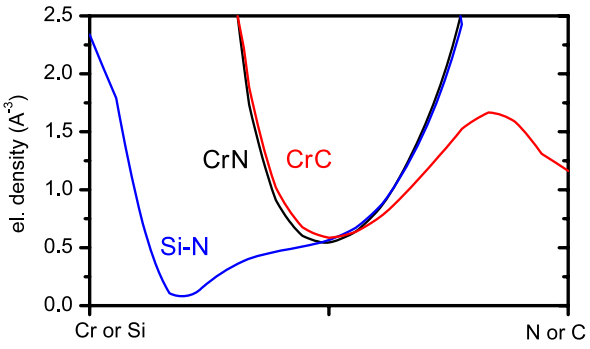

Figure 8. Charge density along the CrN bond (black line), CrC bond in the $CrC_{25}N_{75}$ material (red line), and SiN bond in the $Cr_{75}Si_{25}N_{75}$ material (blue line).

It can be seen that the CrC bond exhibits similar features to CrN, with a minimal value close to 1/2 the bond length. In the case of CrN, the value of the minimum is slightly higher, and closer to the C/N site (despite the higher N electronegativity). The figure confirms that the extra valence electron of N contributes to a high electron density close to the atom core (due to the formation of 2-electron 'lonepairs'),

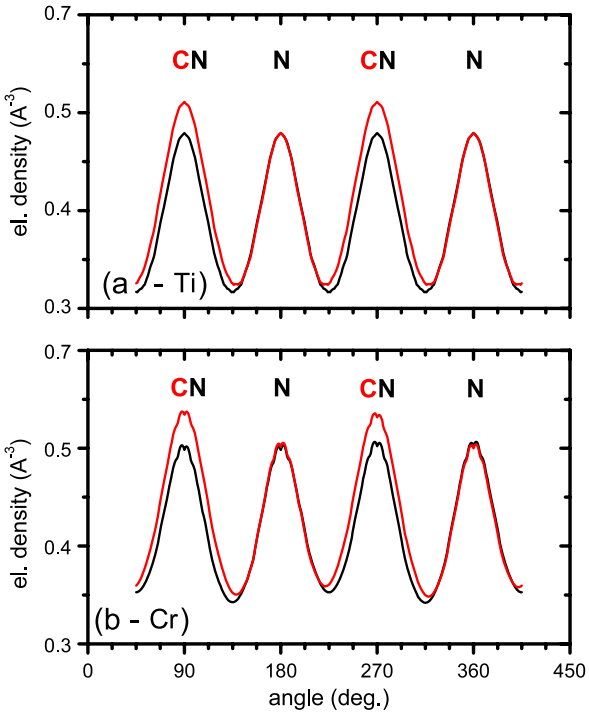

Figure 9. Charge density around Ti (panel (a)) and Cr (panel (b)) along a circle in the xy plane, with a radius equal to 1/2 of a bonding length (1/4 of a lattice constant). Angles of $n \times 90°$ correspond to directions to the nearest neighbor atoms in the circle plane. Each panel shows the charge density for pure metal nitride (black line), and a metal nitride with 12.5% of C, in a C-rich plane with 25% of C (red line). In panel (b), neighbor atoms at positions 90° and 180° are in a layer with the same spin polarization as the central atom and vice versa.

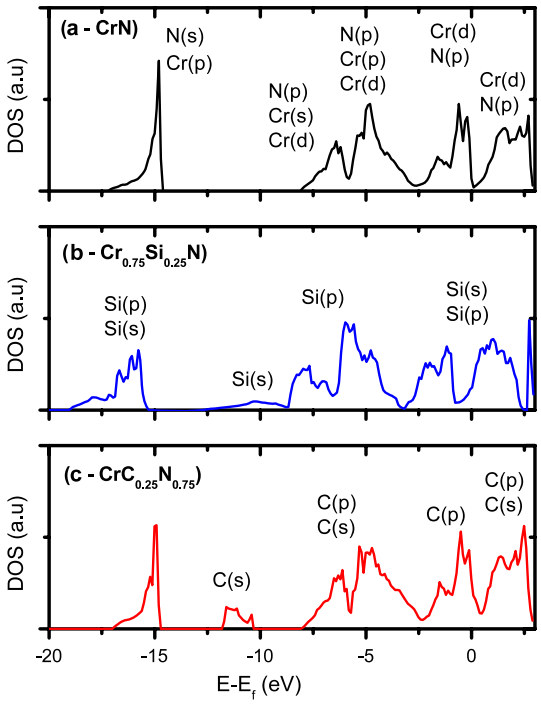

Figure 10. Density of states (DOS) of the CrN (panel (a)), $Cr_{75}Si_{25}N$ (panel (b)) and $CrC_{25}N_{75}$ (panel (c)) materials in the AFM configuration. States exhibiting a higher contribution to individual peaks are denoted by a higher position in the corresponding list (column) of states.

rather than to interatomic bonding. This finding is similar to what has been obtained for TiN and TiC bonds [30]. On the other hand, although Si is generally more prone to form covalent bonds than Ti, the directional bonding is in fact less pronounced in the case of the SiN bond (note also the metal status of the fcc-SiN, with both Si 3s, 3p and N 2s, 2p states at the Fermi level). This is in agreement with the larger changes of $M_{1-x}Si_xN$ characteristics, compared to the changes of MC_xN_{1-x} characteristics, with increasing x.

Figure 9 shows the distribution of electron density around metal atoms along a circle in the xy plane with a high C density, with a radius equal to 1/2 of the bonding length (1/4 of the lattice constant). The figure shows that apart from the higher electron density of $CrC_{25}N_{75}$ compared to $TiC_{25}N_{75}$, due to the extra Cr valence electrons, both materials exhibit similar electron distributions around the interatomic linkages as well as similar effect due to C incorporation on the distributions. In the case of $CrC_{25}N_{75}$, there are slight differences in the bonds between FM layers with the same, and with the opposite, Cr magnetization directions (N or C atoms, although with a little magnetization on their own, are for this purpose associated with the magnetization direction of the ferromagnetic layer they lie in). These differences include (1) deeper minima in the directions perpendicular to the FM layers (for both CrN and $CrC_{25}N_{75}$), and (2) larger (by 20%) increases in electron densities at half of the CrC bond length (resulting from the replacement of N by C) for CrC bonds between layers with the same Cr magnetization. The latter effect can be understood as a consequence of the fact that the C magnetization has an opposite sign to 4 out of the 6 corresponding nearest Cr neighbors (see table 1).

The effect of Si or C incorporation on the AFM CrN electronic structure (density of states, DOS) is shown in figure 10. The most distinctive feature is the behavior of the narrow gap at the Fermi energy (see figure 10(a)), which is characteristic of (pure) CrN [50]. Firstly, the position of the gap is shifted below the Fermi level as a result of Si addition (see figure 10(b)), and to energies above the Fermi level as a result of C addition (see figure 10(c)). Secondly, the pseudogap itself becomes less pronounced (DOS at its bottom increases) as a result of both Si and C addition. This is in agreement with the quantitatively decreasing effect of the AFM ordering resulting from Si or C incorporation shown above (see section 3.2), which for pure CrN leads to a large band splitting and to pseudogap formation [50]. The trend shown can be used to control characteristics such as the optical gap, studied so far only for pure CrN (0.7 eV [19]).

4. Conclusions

We systematically studied the properties of (Cr/Ti)SiN and (Cr/Ti)CN alloys of various compositions ([Si] up to 12.5% and [C] up to 50%) and various distributions of atoms in the lattice by *ab initio* calculations. The modeling approach allowed us to predict the lattice constant, bulk modulus,

elastic tensor, shear modulus, Young's modulus, Poisson's ratio, magnetization and electronic structure, and to determine the preference towards the cubic/orthorhombic structural transformation. We found a very good agreement between both experimental and theoretical data reported previously and our values for TiN ($a_0 = 4.249$ Å, $B = 274$ GPa, $G_{RV} = 191$ GPa, $C_{11} = 584$ GPa, $C_{12} = 119$ GPa, $C_{44} = 167$ GPa, $E_{RV} = 464$ GPa and $\nu_{RV} = 0.22$). Using this model validation we determined reliable results for CrN ($a_0 = 4.156$ Å, $B = 241$ GPa, $G_{RV} = 153$ GPa, $C_{11} = 502$ GPa, $C_{12} = 111$ GPa, $C_{44} = 130$ GPa, $E_{RV} = 379$ GPa and $\nu_{RV} = 0.24$), where the spectrum of experimental result is rather broad. The elastic constants of CrC_xN_{1-x} (increasing B and constant G_{RV}, E_{RV} and ν_{RV}) do not exhibit any decrease due to the C addition, contrary to the elastic constants of TiC_xN_{1-x} (decreasing B and ν_{RV} and an extremal behavior of G_{RV} and E_{RV}). The elastic constants of $Cr_{1-x}Si_xN$, although exhibiting qualitatively the same dependence on x as that of $Ti_{1-x}Si_xN$ (decreasing B, G_{RV}, E_{RV} and increasing ν_{RV}), change quantitatively much more slowly.

The results show the importance of CrN magnetization, and they constitute a number of experimentally testable predictions of the differences between the trends exhibited by chromium and titanium nitrides. In particular, the differences between the evolution of the elastic constants can be explained by a decreasing CrN magnetization resulting from not only the Si addition, but also the C addition. The related (AFM CrN)-specific electronic phenomena include (1) differences in electron density between FM layers with the same magnetization/between FM layers with the opposite magnetization/in the FM layers, and (2) changes in both the significance and position of the CrN pseudogap resulting from C or Si addition. We provide formulae for dependence of the $(Cr/Ti)C_xN_{1-x}$ cubic lattice constant on C content, and find a weakening of the CrN preference towards the cubic/orthorhombic structural transformation due to the Si or C addition. Moreover, we predict an improved low-temperature adhesion (due to a lower compressive stress) of CrC_xN_{1-x} at higher C content resulting not only from changes in preference towards the cubic/orthorhombic structural transformation, but also from the lower AFM/PM cubic lattice constant misfit.

The results presented allow one to tailor the material characteristics of wear-resistant and/or oxidation-resistant ternary metal nitrides of the required elastic, electronic or adhesive characteristics for various protective, decorative, tribological or other advanced applications.

Acknowledgments

This work was supported in part by grants from the Natural Sciences and Engineering Research Council (NSERC) of Canada. Computational resources were provided by the Réseau québécois de calcul de haute performance (RQCHP).

References

[1] Lengauer W, Binder S, Aigner K, Ettmayer P, Guillou A, Debuigne J and Groboth G 1995 *J. Alloys Compounds* **217** 137
[2] Yang Q, Lengauer W, Koch T, Scheerer M and Smid I 2000 *J. Alloys Compounds* **309** L5
[3] Holleck H 1986 *J. Vac. Sci. Technol.* A **4** 2661
[4] Richter V, Beger A, Drobniewski J, Endler I and Wolf E 1996 *Mater. Sci. Eng.* A **209** 353
[5] Warcholinski B, Gilewicz A, Kuklinski Z and Myslinski P 2009 *Vacuum* **83** 716
[6] Lackner J M, Waldhauser W, Major B, Morgiel J, Major L, Takahashic H and Shibayamac T 2006 *Surf. Coat. Technol.* **200** 3644
[7] Haug F J, Schwaller P, Wloka J, Patscheider J, Karimi A and Tobler M 2004 *J. Vac. Sci. Technol.* A **22** 1229
[8] Bendavid A, Martin P J, Cairney J, Hoffman M and Fischer-Cripps A C 2005 *Appl. Phys.* A **81** 151
[9] Jedrzejowski P, Amassian A, Bousser E, Klemberg-Sapieha J E and Martinu L 2006 *J. Appl. Phys. Lett.* **88** 071915
[10] Flink A, Larsson T, Sjolen J, Karlsson L and Hultman L 2005 *Surf. Coat. Technol.* **200** 1535
[11] Choi J B, Cho K, Kim Y, Kim K H and Song P K 2003 *Japan. J. Appl. Phys.* **42** 6556
[12] Benkahoul M, Robin P, Gujrathi S C, Martinu L and Klemberg-Sapieha J E 2008 *Surf. Coat. Technol.* **202** 3975
[13] Martinez E, Sanjines R, Banakh O and Levy F 2004 *Thin Solid Films* **447/448** 332
[14] Sandu C S, Sanjines R, Benkahoul M, Medjani F and Levy F 2006 *Surf. Coat. Technol.* **201** 4083
[15] Nose M, Chiou W A, Zhou M, Mae T and Neshii M 2002 *J. Vac. Sci. Technol.* A **20** 823
[16] Houska J, Klemberg-Sapieha J E and Martinu L 2009 *Surf. Coat. Technol.* at press (doi:10.1016/j.surfcoat.2009.04.021)
[17] Zhang R F and Veprek S 2007 *Phys. Rev.* B **76** 174105
[18] Corliss L M, Eliott N and Hastings J 1960 *Phys. Rev.* **117** 929
[19] Gall D, Shill C S, Haasch R T, Petrov I and Greene J E 2002 *J. Appl. Phys.* **91** 5882
[20] Lambrecht W R L, Miao M S and Lukashev P 2005 *J. Appl. Phys.* **97** 10D306
[21] Soriano L, Abbate M, Pen H, Prieto P and Sanz J M 1997 *Solid State Commun.* **102** 291
[22] Constantin C, Haider M B, Ingram D and Smith A R 2004 *Appl. Phys. Lett.* **85** 6371
[23] Gilman J J, Cumberland R W and Kaner R B 2006 *Int. J. Refract. Met. Hard Mater.* **24** 1
[24] Grossman J C, Mizel A, Cote M, Cohen M L and Louie S G 1999 *Phys. Rev.* B **60** 6343
[25] Hultman L, Bareno J, Flink A, Soderberg H, Larsson K, Petrova V, Oden M, Greene J E and Petrov I 2007 *Phys. Rev.* B **75** 155437
[26] Jhi S-H and Ihm J 1997 *Phys. Rev.* B **56** 13826
[27] Jhi S-H, Ihm J, Louie S G and Cohen M L 1999 *Nature* **399** 132
[28] Ivashchenko V I, Turchi P E A, Gonis A, Ivashchenko L A and Skrynski P L 2006 *Metall. Mater. Trans.* A **37** 3391
[29] Marlo M and Milman V 2000 *Phys. Rev.* B **62** 2899
[30] Zaoui A, Kacimi S, Bouhafs B and Roula A 2005 *Physica* B **358** 63
[31] Mayrhofer P H, Music D, Reeswinkel Th, Fus H G and Schneider J M 2008 *Acta Mater.* **56** 2469
[32] Hohenberg P and Kohn W 1964 *Phys. Rev.* B **136** 864
[33] Kohn W and Sham L 1965 *Phys. Rev.* A **140** 1133
[34] Baroni S, Dal Corso A, de Gironcoli S, Giannozzi P, Cavazzoni C, Ballabio G, Scandolo S, Chiarotti G, Focher P, Pasquarello A, Laasonen K, Trave A, Car R, Marzari N and Kokalj A http://www.pwscf.org
[35] CPMD, Copyright IBM Corp 1990–2008, Copyright MPI fuer Festkörperförschung Stuttgart 1997–2001
[36] Laasonen K, Car R, Lee C and Vanderbilt D 1991 *Phys. Rev.* B **43** 6796
[37] Perdew J P, Burke K and Ernzerhof M 1996 *Phys. Rev. Lett.* **77** 3865

[38] Alling B, Marten T, Abrikosov I A and Karimi A 2007 *J. Appl. Phys.* **102** 044314
[39] Era H, Ide Y, Nino A and Kishitake K 2005 *Surf. Coat. Technol.* **194** 265
[40] Gall D, Shin C S, Spilla T, Oden M, Senna M J N, Greene J E and Petrov I 2002 *J. Appl. Phys.* **91** 3589
[41] Mehl M 1993 *Phys. Rev.* B **47** 2493
[42] Zhu R, Pan E, Chung P W, Cai X, Liew K M and Buldum A 2006 *Semicond. Sci. Technol.* **21** 906
[43] Zotov N and Ludwig A 2008 *Intermetallics* **16** 113
[44] Ellaway S W and Faux D A 2002 *J. Appl. Phys.* **92** 3027
[45] Maxwell A S, Owen-Jones S and Jennett N M 2004 *Rev. Sci. Instrum.* **75** 970
[46] Chen H Y, Tsai C J and Lu F H 2004 *Surf. Coat. Technol.* **184** 69
[47] Wiklund U, Bromark M, Larsson M, Hedenqvist P and Hogmark S 1997 *Surf. Coat. Technol.* **91** 57
[48] Barata A, Cunha L and Moura C 2001 *Thin Solid Films* **398** 501
[49] Baragetti S, LaVecchia G M and Terranova A 2003 *Int. J. Fatigue* **25** 1229
[50] Filippetti A, Pickett W E and Klein B M 1999 *Phys. Rev.* B **59** 7043